Research Article **Open Access**

Jiangguo Liu*, Farrah Sadre-Marandi, Simon Tavener, and Chaoping Chen

Curvature Concentrations on the HIV-1 Capsid

DOI 10.1515/mlbmb-2015-0003
Received December 7, 2014; accepted June 8, 2015

Abstract: It is known that the retrovirus capsids possess a fullerene-like structure. These caged polyhedral arrangements are built entirely from hexagons and exactly 12 pentagons according to the Euler theorem. Viral capsids are composed of capsid proteins, which create the hexagon and pentagon shapes by groups of six (hexamer) and five (pentamer) proteins. Different distributions of these 12 pentamers result in icosahedral, tubular, or conical shaped capsids. These pentamer clusters introduce declination and hence curvature on the capsids. This paper provides explicit and quantitative characterization of curvature on virus capsids. The concept of curvature concentration is also introduced. For the HIV (5,7)-cone, it is shown that the curvature concentration at the narrow end is about **at least four times higher** than that at the broad end. Our modeling results about curvature concentrations on HIV-1 capsids echo the results in the literature that the pentamers are in the regions with the highest stress, although the connection between the two approaches (curvature concentration and stress) is to be explored. This also leads to a conjecture that *"HIV-1 capsid narrow end may close last during maturation but open first during entry into a host cell"*.

Keywords: capsid; cone; curvature; hexamer; HIV-1; pentamer

1 Introduction

The human immunodeficiency virus type 1 (HIV-1) is a retrovirus that causes the acquired immunodeficiency syndrome (AIDS). Because of the exceptionally high mortality rates due to AIDS and the peculiar structure of HIV-1 virions, HIV-1 virus is an active research area, see, e.g., [5, 14, 28, 41] and references therein.

Immature HIV-1 virions bud on the plasma membrane of an infected host cell and then undergo the maturation process [14, 21], during which capsid proteins form a conical shell that protects the viral RNA genome and performs essential functions in the virus life cycle. While significant progresses have been made with regards to understanding the assembly mechanism and structure of the HIV-1 and more general viral capsids [1, 8–11, 16, 17, 29–31, 35, 36, 41], there are yet many questions to be answered.

HIV-1 conical cores along with other virus capsids are best described by a fullerene-like structure. Generally speaking, this structure is a cage-like macromolecule that has a simple 3-valent, n-vertex polyhedral surface. Geometrically, such a capsid forms a closed surface, consisting of hexagons and exactly 12 pentagons, according to the Euler theorem. The capsid proteins (CA) join together to create the hexagon and pentagon shapes by grouping six (hexamer) and five (pentamer) proteins. The capsid encloses the viral RNA or DNA, providing a protective barrier.

***Corresponding Author: Jiangguo Liu:** Department of Mathematics, Colorado State University, Fort Collins, CO 80523-1874, USA, E-mail: liu@math.colostate.edu
Farrah Sadre-Marandi: Department of Mathematics, Colorado State University, Fort Collins, CO 80523-1874, USA, E-mail: sadre@math.colostate.edu
Simon Tavener: Department of Mathematics, Colorado State University, Fort Collins, CO 80523-1874, USA, E-mail: tavener@math.colostate.edu
Chaoping Chen: Department of Biochemistry and Molecular Biology, Colorado State University, Fort Collins, CO 80523-1870, USA, E-mail: Chaoping.Chen@ColoState.edu

Small-size viral capsids tend to conform to the preferred icosahedral symmetry [7, 20]. This symmetry allows the 12 pentamer groups to be evenly placed on the surface of a sphere. Although most viral capsids follow the fullerene-like structure, not all virus capsids follow the icosahedral symmetry. Tubular (spherocylinder) viral capsids have been observed for Cowpea Chlorotic Mottle Virus and Alfalfa Mosaic Virus, among others. The HIV-1 capsid is cone-shaped and composed of exactly 12 pentamers and approximately 218 hexamers [5, 31, 37]. The murine leukemia virus (MuLV) and Rous sarcoma virus (RSV) also exhibit asymmetry or irregularity in their capsid structures [18].

The cone angle of the HIV-1 capsid has been measured in experiments by dehydrating the core of a virus-like particle (VLP) onto a carbon grid [11]. It is found that the angle was quantified into the five allowed values prescribed by the Euler formula

$$\sin(\theta/2) = 1 - P/6, \tag{1}$$

where θ is the cone angle and P is the number of pentamers at the narrow end of the cone. The five angle values (and the corresponding P values) are $\theta = 112.9^\circ (P = 1)$, $\theta = 83.6^\circ (P = 2)$, $\theta = 60^\circ (P = 3)$, $\theta = 38.9^\circ (P = 4)$, $\theta = 19.2^\circ (P = 5)$. For convenience, we name these cones as (1,11)-, (2,10)-, (3,9)-, (4,8)-, (5,7)-patterns. It is also found that the viral core and most synthetic cones exhibited cone angles of approximately 19 degrees [11], in other words, most HIV-1 cones are in the (5,7)-pattern, but (4,8)-cones and other unusual types of VLPs have also been observed in experiments [2–4].

Recently, the cone structure of the HIV-1 capsid has been intensively investigated. It is suggested in [6] that the asymmetry and quasi-equivalence exhibiting in conic and tubular capsids are related to the hinge between the C-terminal domain (CTD) and N-terminal domain (NTD) of the capsid protein. In [37], it is presented that the 12 pentamers introduce sharp declinations on the HIV-1 capsid. A line of hexamers connecting two declinations is presented to illustrate the continuously varying curvature, as shown Figure 4. Dihedral angles along this line are also calculated. These dihedral angles between two subunits (hexamer/hexamer or hexamer/pentamer) are defined as bite angles. It is discussed in [14] that the bite angle between adjacent hexamers vary from around 135° between two hexamers connected to the same pentamers at either end of the HIV-1 cone to around 180° in the more flat region in the middle of the cone. In [14], there is also examination on the different angles between the subunits in CA pentamers or hexamers and the approximate pivot point for rotations. It is concluded in [31] that the rigid-body rotations around these assembly interfaces seem to be sufficient for explaining the curvature variation on the HIV-1 cone. It is also concluded in [41] that incorporation of CA pentamers into the surface hexameral lattice induces acute surface curvature. These studies deepen our understanding of viral capsid structure and viral assembly mechanism and motivate inhibitor for the formation of critical CA-CA interfaces in the capsid assembly [13].

This paper presents an explicit and ease-to-use approach for quantitative characterization of curvatures on virus capsids. Furthermore, the concept of curvature concentration is introduced and this quantity is calculated for the narrow and broad ends of HIV-1 conical capsids. For HIV (5,7)-, (4,8)- conical capsids, the results in this paper show that the narrow end always has the highest curvature concentration, which is an indication that the narrow end on the HIV-1 capsid is a region with the largest stress.

2 Mathematical Background: Curvature and Discrete Curvature

To understand curvatures on a surface, we need the concept of curvatures on a curve. In three-dimensional space, the curvature of a curve at a given point is a measure of how fast the curve changes its direction at that point. A formal mathematical definition for curvature is given by

$$\kappa = \left| \frac{d\vec{T}}{ds} \right|,$$

where $\vec{T}$ is the unit tangent vector and s is the arc length [32].

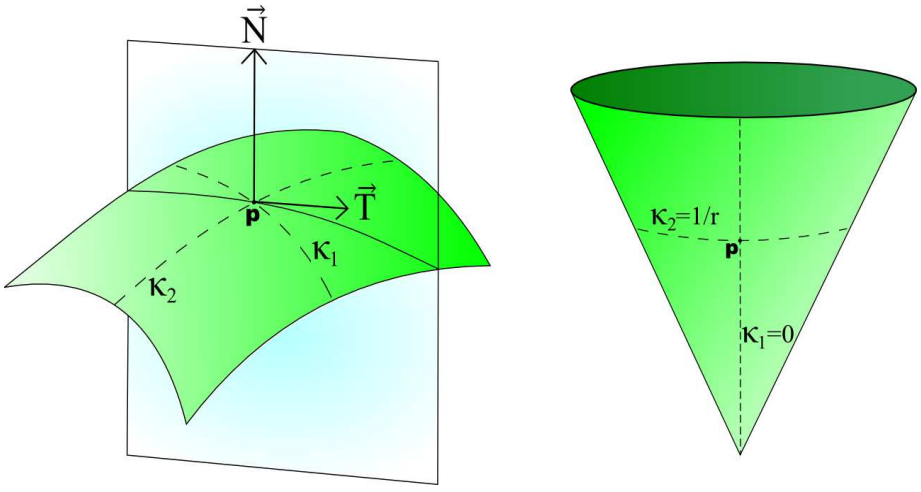

Figure 1: *Left*: There are two principal curvatures κ_1 and κ_2 at a point p on a smooth surface. *Right*: For a point on a conic surface, the minimum principal curvature is $\kappa_1 = 0$ whereas the maximum principal curvature is $\kappa_2 = 1/r$ with r being the radius of the circular section on which the point is located.

2.1 Continuous Curvatures on a Smooth Surface

Let M be a smooth surface and p be a point on M. The curvatures are characterized and quantified by the shape operator S, defined as

$$S = \cup\{\pm S_p : p \in M\}, \qquad S_p(\vec{\mathbf{u}}) = -D_{\vec{\mathbf{u}}}\vec{N}(p),$$

where $\vec{N}$ is the unit normal vector field defined in an open neighborhood of the point p on the given surface M, $\vec{\mathbf{u}}$ is any tangent vector to M at p, namely, a tangent vector to a curve that passes through the point p and is entirely on the surface M. Note that $S_p(\vec{\mathbf{u}})$ defines the negative directional derivative of M at p along the vector $\vec{\mathbf{u}}$. Intuitively, $S_p(\vec{\mathbf{u}})$ explains how the surface M "curves" around the point p. The shape operator of M at p derived from $-\vec{\mathbf{u}}$ is $-S_p$, since it essentially reverses only the direction. Therefore, the shape operator of M is the union of all S_p at the given point p on M [32]. For a non-planar surface, the **Gaussian curvature** is given by the determinant of the operator S.

The principal curvatures of a surface at a given point are the two eigenvalues of the shape operator S discussed above. Denoted as κ_1 and κ_2, the principal curvatures measure the maximum and minimum bending of the surface at a given point, as shown in Figure 1. Mathematically, the Gaussian curvature is $K = \kappa_1\kappa_2$, the product of the two principal curvatures. These principal curvatures can also be used to define other terms, e.g., the *mean curvature* $\frac{1}{2}(\kappa_1 + \kappa_2)$.

For example, the Gaussian curvature of a plane at any point is zero as the plane will not bend in any direction, that is, $\kappa_1 = \kappa_2 = 0$ and hence $K = \kappa_1\kappa_2 = 0$. Cylinders and cones also have zero Gaussian curvature, since the minimum principal curvature $\kappa_1 = 0$ in each shape. The case for a cone is illustrated in the right panel of Figure 1.

For a smooth surface M, the Gauss-Bonnet Theorem (see [32]) asserts that the integral of the Gaussian curvature on the surface is equal to 2π times the Euler characteristic:

$$\iint_M K(p)dp = 2\pi\chi_M. \tag{2}$$

2.2 Triangulation and the Euler Characteristic of a Polyhedral Surface

In the discrete setting, a smooth surface is replaced by a polyhedral surface. The concept of the discrete Gaussian curvature on a polyhedral surface is based on the triangulation of such a surface. Triangulation, in this

case, is equivalent to the idea of tiling, see [23, 24], in which the tiles or subsections within one polygon are related by the theory of quasi-equivalence. For convenience, we assume each tile is equivalent, resulting in similar triangles within each hexagon or pentagon along the polyhedral surface. Since each polygon is cut into similar triangles, we call this process triangulation.

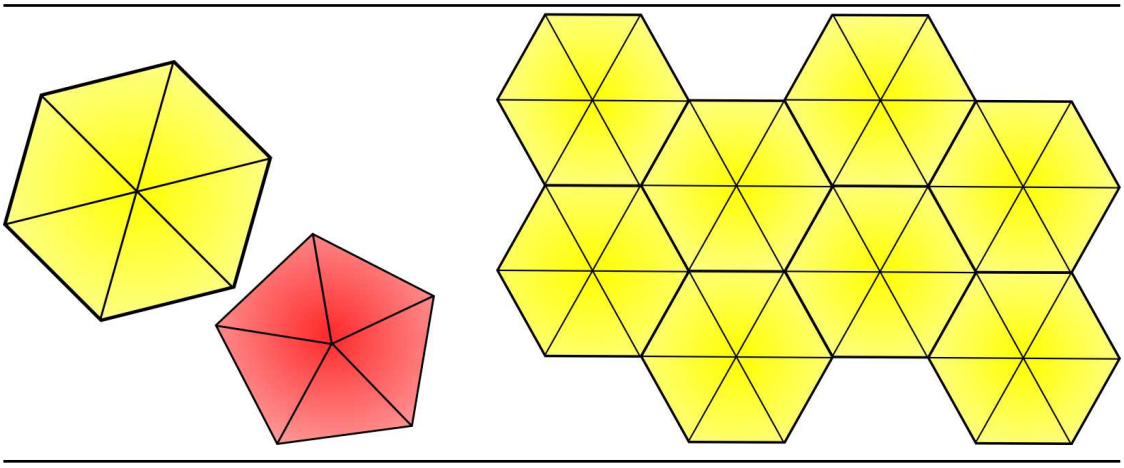

Figure 2: *Left*: A hexagon (in color yellow) and a pentagon (in color red) are each cut by similar triangles. *Right*: A hexagonal lattice is triangulated by cutting each hexagon into six equilateral triangles, all sharing the vertex in the center.

Consider a polyhedral surface as a set of polygons (in the space) joined together at their edges with varying dihedral angles. The most natural way for cutting a polyhedral surface into subsections is to divide the non-triangular shape into the smallest amount of similar triangles. For example, to triangulate a hexagon, one would cut it into six equal pieces, with a common vertex at the center of the hexagon, as shown in Figure 2 (left panel). Pentagons can be cut in a similar fashion, with five similar triangles having a common vertex at the center of each pentagon, see also the left panel of Figure 2.

Let M be a polyhedral surface. Denote by V the number of vertices, E the number of edges, and F the number of faces. The Euler characteristic of a closed polyhedral surface is given as $\chi_M = V - E + F$, regardless of how the surface is bent. Any closed convex polyhedral surface has an Euler characteristic $\chi_M = 2$, see [23, 32]. This characteristic is independent of the choice of subsections, triangles, or tiles, since it is assumed each polygon is a planar object.

2.3 Discrete Gaussian Curvature on a Polyhedral Surface

In the discrete setting, the Gauss-Bonnet Theorem (see [32]) holds analogously

$$\sum_{v\in D} K_v = 2\pi\chi_M; \qquad K_v = 2\pi - \sum_i \theta_i, \tag{3}$$

where D is a triangulated region on a given polyhedral surface M, v is a vertex in D, and θ_i are the interior angles at v. Each θ_i is an angle of a triangle adjoined at v. K_v is called the *angle defect* at v, which describes the **discrete Gaussian curvature** at the point.

Viral capsids are examples of closed convex polyhedral surfaces. Their Euler characteristic is $\chi = 2$, and so the sum of the discrete Gaussian curvatures is 4π. For icosahedral capsids, the curvature is distributed uniformly over the capsid due to its spherical-like shape. Non-icosahedral capsids do not share this property. A question then arises: how is the total curvature of 4π distributed throughout the capsid?

3 Curvature Concentrations on the HIV-1 Conical Capsid

Many known viral capsids have a fullerene-like structure, which is a caged polyhedral surface composed of coating proteins or subunits grouped as hexamers and pentamers (6 and 5 proteins respectively). The number of hexamers varies for each capsid, depending on the size of the capsid. However, the number of pentamers always equals 12. This specific number of pentamer groups is required by the Euler Theorem to guarantee closure with no holes.

Some viral capsids have icosahedral or cylindrical symmetry. For the former, the pentamers are evenly spaced. For the latter, the pentamers are split into a (6,6)-pattern: 6 pentamers in the bottom, 6 pentamers in the top, and a large number of hexamers between the two ends.

HIV-1 is a virus that has a cone shape, mostly in the (5,7) pattern, that is, 5 pentamers at the narrow end and 7 pentamers at the broad end. In [3], it is demonstrated that HIV-1 VLPs could have a larger cone angle resulting in a (4,8)-cone shape. Mathematically, there are five possible cones: (5,7), (4,8), (3,9), (2,10), (1,11). However, extreme distributions such as the (2,10)- and (1,11)-cones are rarely seen in the nature [15].

For icosahedral viral capsids with triangulation number $T > 1$, pentamers are isolated, each surrounded by a ring of hexamers. Isolation of pentamers is also suggested for non-icosahedral viral capsids by the end-diameter measurements in [2–5, 11, 31] and the HIV-1 capsid modeling efforts in [26, 33] as well. Carbon fullerene structures also exhibit pentagons surrounded by a ring of hexagons, since this is a more stable configuration [15]. Assuming pentamers are isolated and considering triangulation of the hexamers and pentamers in the most natural way lead to *only two possible cases* for curvature calculations, due to the consistent interior angles in each polygon.

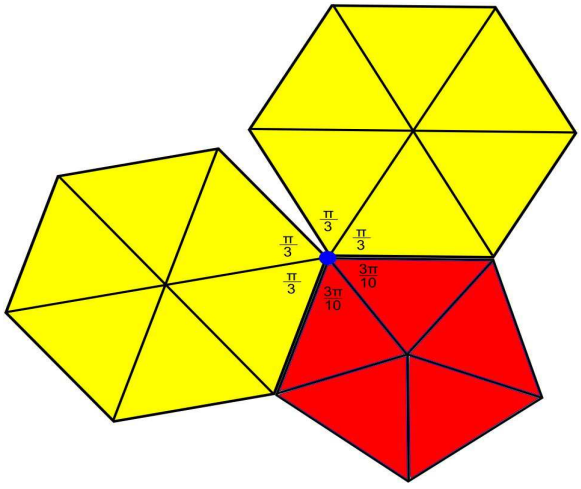

Figure 3: *Case 1*: A pentamer is surrounded by hexamers. Around a pentamer vertex, each triangle inside the pentamer has an interior angle $\theta = 3\pi/10$ whereas each triangle inside the hexamers has an interior angle $\theta = \pi/3$.

Case 1. The first case occurs when a vertex v of a pentamer P is surrounded by two hexamers H, as shown in Figure 3. The triangulation produces six equilaterial triangles for each hexamer and five similar triangles for the pentamer. At the very vertex, there are a total of six interior angles, four from the hexamers and two from the pentamer triangulation. The interior angles of the triangles in the hexamers have values $\theta_i = \pi/3$ for $i = 1, 2, 3, 4$. The interior angles in the pentamers have values $\theta_i = 3\pi/10$ for $i = 5, 6$.

Then the angle defect or the discrete Gaussian curvature at v is given by

$$K_v(P) = 2\pi - \sum_i^6 \theta_i = 2\pi - 4\left(\frac{\pi}{3}\right) - 2\left(\frac{3\pi}{10}\right) = \frac{\pi}{15}. \tag{4}$$

Notice that the curvature calculation will be the same for each vertex of the pentamers P, since each vertex of P is also connected to $2H$ with the same triangulation. Each of the five vertices of P contributes a curvature of $\pi/15$, so the total discrete Gaussian curvature for the entire pentamer P is $\pi/3$.

Case 2. The second case occurs when a hexamer is surrounded by six other hexamers. Connecting the hexamers creates a flat surface (plane), as shown in Figure 2. Considering the same triangulation used in case one, the interior angles at each vertex v are given by $\theta_i = 60^\circ = \pi/3$ for $i = 1, 2, 3, 4, 5, 6$. The discrete Gaussian curvature at v is then

$$K_v(H) = 2\pi - \sum_{i}^{6} \theta_i = 2\pi - 6\frac{\pi}{3} = 0. \tag{5}$$

Given exactly 12 pentamers and N_H hexamers, the total discrete Gaussian curvature of the caged cone is

$$12 * 5 * K_v(P) + N_H * 6 * K_v(H) = 4\pi,$$

which agrees with the discrete version of the Gauss-Bonnet Theorem (3).

For a cone-shaped capsid, the total curvature is independent of the number of hexamers in the cone and the curvature is nonzero only at pentamer positions. This implies the position of each pentamer is related to a location of high curvature on the capsid, introducing sharp declinations on the capsid as observed in [31, 37].

3.1 Curvature Concentrations on the (5,7)-Cone

Consider the HIV-1 conical capsid as a polyhedral surface M, consisting of hexamers H and pentamers P. We assume that each vertex of P is surrounded by a pentamer and two hexamers.

The (5,7)-pattern has been widely reported in experimental observations. This means 5 pentamers at the narrow end of an HIV-1 cpasid and 7 pentamers at the broad end of the capsid. This is the case when the capsid has a cone angle 19.2° [2–4, 11].

The total discrete curvature of the broad end (or the top) is $K_{7P} = 7\pi/3$, whereas the total discrete curvature of the narrow end (or the bottom) is $K_{5P} = 5\pi/3$. The middle region of the cone is assumed to have only hexamers, so the total discrete curvature of this part is zero. This could be better understood when considering the middle region of the HIV-1 capsid as a right cone. The principal curvatures at any point on the right cone are given by $\kappa_1 = 0$ and $\kappa_2 = 1/r$ (r is the radius of the circular section on which the point is located), as shown in Figure 1. The Gaussian curvature at any point on a right cone is zero.

Another useful metric is the curvature concentration, i.e., curvature per area on a given surface.

General Formulas. To calculate the curvature concentration, the sum of the areas of the hexamers and pentamers in each region (the narrow end or the broad end) is considered. For the (5,7)-cone, there are 5 pentamers in the narrow end and 7 pentamers in the broad end. Assume

(A1). These pentamers are isolated;
(A2). For each end, each vertex of a pentamer is surrounded by the pentamer and two hexamers;
(A3). There are H_n hexamers in one particular end (narrow end or broad end);
(A4). a is the side length of pentamers or hexamers.

Then direct mathematical calculations yield the formulas for surface area (SA) as follows

$$SA_{5P}(a, H_n) = a^2\left(H_n\frac{3\sqrt{3}}{2} + \frac{5}{4}\sqrt{5(5+2\sqrt{5})}\right), \tag{6}$$

$$SA_{7P}(a, H_n) = a^2\left(H_n\frac{3\sqrt{3}}{2} + \frac{7}{4}\sqrt{5(5+2\sqrt{5})}\right). \tag{7}$$

Parameter Estimates. The overall height of an HIV-1 capsid was found to be 119 ± 11nm [3], and the mean diameters of the broad and narrow ends are 56nm and 27nm, respectively [4]. Using the measurements reported in [3, 5, 31, 37], it is estimated that

- 4% of the hexamers lay at the narrow end;
- 36% of the hexamers are at the broad end;
- the remaining 60% are in the middle region;

with an average of 218 hexamers in each capsid.

Recent cryo-EM results [41] indicate a larger diameter at the narrow end, with an estimate of 6% of the hexamers at the narrow end, 33% at the broad end, and 61% in the middle region, with an average of 216 hexamers.

The diameter of a hexameric unit was found to be approximately 9.8nm with a 3.2nm spacing between units in VLPs [3]. Therefore, for the fullerene-like structure model, it is assumed each subunit (pentamer or hexamer) has a side length 6.5nm.

Calculations. For the narrow end of an HIV-1 capsid, the surface area is calculated using formula (7), with a range

$$SA_{5P}(6.5, H_n) \approx 1,460 \pm 219\text{nm}^2.$$

Similarly, the surface area of the broad end is estimated as

$$SA_{7P}(6.5, H_n) \approx 8,796 \pm 384\text{nm}^2.$$

The curvature concentration is defined as the ratio of the discrete Gaussian curvature per surface area in each region. For the broad and narrow ends, we have respectively curvature concentrations

$$C_{K_{7P}} \approx 8.34 \times 10^{-4}, \qquad C_{K_{5P}} \approx 3.59 \times 10^{-3}.$$

These results show that $C_{K_{5P}}$ **is at least four times higher than** $C_{K_{7P}}$**,** that is, the curvature concentration at the narrow end is at least four times higher than that at the broad end.

3.2 Curvatures on (4,8)- and Other Type Cones

As discussed in the previous sections, there are five possible cone angles for a cone composed of only hexamers and pentamers, according to the Euler formula. Although 19.2° is the most common cone angle for HIV-1 cores, larger cone angles between 30° and 40° have also been reported in experimental data [2, 3, 11]. This implies that HIV-1 cores could form into a cone with $4P$ at the narrow end and $8P$ at the broad end. Both (4,8)- and (3,9)-cones have been seen in graphite nanocones, although it is thought (2,10)- and (1,11)-cones will not form, due to the high strain at the narrow end [15].

Based on the same assumptions (A1)-(A4) listed in the previous subsection, the surface areas of the narrow ($4P$) and broad ($8P$) ends of a conic capsid are estimated by adding the surface areas of hexamers and pentamers in each region as follows,

$$SA_{4P}(a, H_n) = a^2 \left(H_n \frac{3\sqrt{3}}{2} + \sqrt{5(5 + 2\sqrt{5})} \right), \tag{8}$$

$$SA_{8P}(a, H_n) = a^2 \left(H_n \frac{3\sqrt{3}}{2} + 2\sqrt{5(5 + 2\sqrt{5})} \right), \tag{9}$$

where again H_n is the number of hexamers in that region and a is the side length of the pentamers or hexamers.

For the (4,8)-cone, based on the above formulas, one has approximations for the surface areas as follows

$$SA_{8P} \approx 8,485\text{nm}^2, \qquad SA_{4P} \approx 1,059\text{nm}^2.$$

Then the curvature concentrations of the broad and narrow ends are respectively

$$C_{K_{8P}} \approx 9.87 \times 10^{-4}, \qquad C_{K_{4P}} \approx 4 \times 10^{-3}.$$

Therefore, $C_{K_{4P}}$ **is at least four times higher than** $C_{K_{8P}}$**.**

Similar calculations can be performed for curvature concentrations of other cone types. As the number of P (pentamers) in the narrow end decreases, the surface area and total curvature for that region will also decrease. As the number of P in the broad end increases, the surface area and total curvature of that region will increase. This shows that the narrow end always has the highest curvature concentration on the HIV-1 capsid and hence may be the "weakest" region in some sense, regardless of the cone angle.

4 Discussion

Relation to Declination. Existing work [12, 25, 31, 37, 39, 40] suggest that the pentamers introduce sharp declinations in the HIV-1 capsid. This agrees with our curvature calculations. These sharp declinations occur because the pentamers are the sources of curvature on the closed capsid. In the middle region of the HIV-1 capsid, the dihedral angles (angles between the hexamer-hexamer planes) vary but are close to 180°.

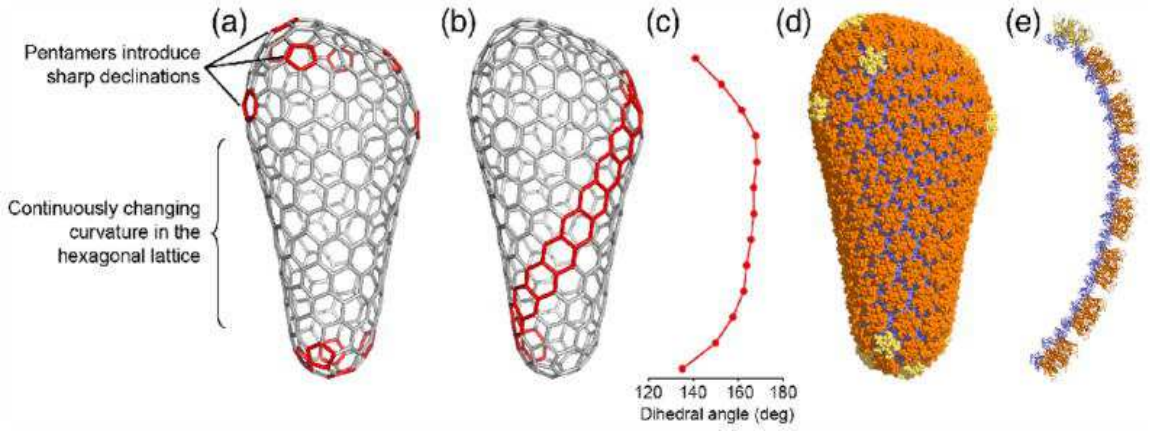

Figure 4: On a caged (5,7)-cone, the 12 pentamers (red) introduce sharp declinations to close the capsid. The graph of the dihedral angles between the hexamers shows measurements close to 180°, implying similarity between the middle region and a rolled plane. **Source**: [37] (with permission from Elsevier for reuse of the figure).

Note that the curvature at a point depends on the interior angles of the triangles meeting there. A dihedral angle in this case is the angle between two triangles in the triangulation of pentamers or hexamers. By the definition of the discrete Gaussian curvature, for the curvature to be 0 at one point, the dihedral angle should be 180° (equivalent to $\kappa_1 = 0$) along one principal direction. For a cone, this direction usually occurs along the edge straight up to the broad end, as shown by the κ_1 dotted line in the right panel of Figure 1.

Conjecture: HIV-1 Narrow End Closed Last But Opened First. The above curvature calculations demonstrate that HIV-1 capsid has positive curvature in the narrow and broad ends but zero curvature in the middle of the cone. *No curvature* in the middle region might mean *no stress*, and hence the middle region may be the first to be formed. This is consistent with the curled sheet model [38] and the assembly mechanisms investigated in [22, 40], which conclude that pentamers are formed later in assembly, due to high stress.

There should be connection between the high curvature concentration in the narrow end and the high stress around pentamers. It has been reported experimentally for P22 and TYMO (turnip yellow mosaic) virus [40] that disassembly is initiated by pentamer release. This is echoed by our curvature results. When capsid becomes thermodynamically unfavorable, regions with high stress or high curvature would be the first to break apart. Recent experimental and modeling studies also show that HIV-1 narrow end might not close, if conditions are unfavorable [38], as shown in Figure 5. This discusion leads to our conjecture: *the narrow*

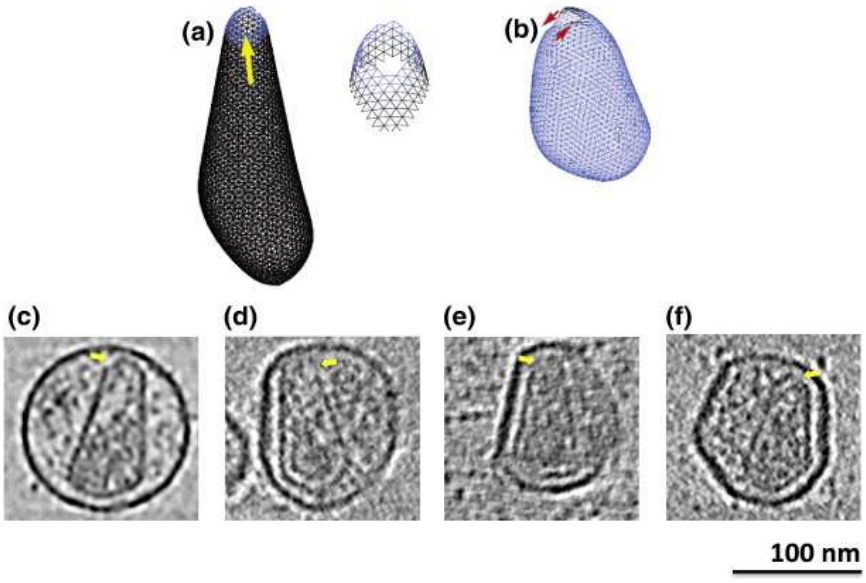

Figure 5: Modeling and experimental results in [38] show that the HIV-1 capsid narrow end might not close, if conditions are unfavorable. **Source**: [38] (with permission from Elsevier for reuse of the figure).

end of the HIV-1 capsid might be closed last during viral maturation but opened first during entry into a host cell. Our future work will explore this conjecture further and the connection between stress and curvature concentration.

More Experimental Data Desired for Other Types of HIV-1 Conical Cores. The majority of the existing work on the HIV-1 cone model focuses on the (5,7)-pattern, even though (4,8)-cones have been observed in experiments [3]. The results in this paper show that the (4,8)-cone has also high contrast of curvature concentrations for the narrow and broad ends. It should be interesting to examine possibility and stability (or instability) of formations for different types of cones. It will be helpful for modeling research on HIV-1 cone structure if more detailed and specific experimental data on different types of cones are available. Typically, both the (5,7)- and the (4,8)-cone statistics get grouped together during averaging. Yet having independent information on the (4,8)- and other types of cones will help identify favorable or unfavorable conditions for formation of HIV-1 cone structure.

Relation of Curvature to Elastic Energy. The modeling research presented in this paper shows that the narrow end of the HIV-1 conical core has the highest curvature concentration for the (5,7)- and (4,8)-patterns. This high curvature concentration is tightly related to the stress and elastic (bending) energy at the narrow/broad ends. Similar conjectures have been analyzed to find out

- To which extent localization of Gaussian curvature depends on elastic stiffness [19];
- The connection among the nonzero spontaneous curvature, the energy of the 12 pentameric declinations, and formation of particular capsid shape [26, 27].

It is important to note that even though the HIV-1 conical capsids may have high stress regions, the conical capsids do not constitute energy minimum structures unless their volume and height are fixed [26]. The bending might be related to the hinge between the CTD and NTD of the CA protein. Studying the excess energy could shed light on HIV-1 conical structure [34]. These are under our investigation and shall be reported in our future work.

Capsids of Other Types of Retroviruses. The concepts and methodology presented in this paper could be applied to other types of viral capsids, e.g., murine leukemia virus (MuLV) and Rous sarcoma virus (RSV) [18]. This is also under our investigation.

Conflict of interest. Author state no conflict of interest.

References

[1] G.D. Bailey, J.-K. Hyun, A.K. Mitra, R.L. Kingston, *A structural model for the generation of continuous curvature on the surface of a retroviral capsid*, J. Mol. Biol., **417**(2012), pp. 212–223.

[2] J. Benjamin, B.K. Ganser-Pornillos, W.F. Tivol, W.I. Sundquist, G.J. Jensen, *Three-dimensional structure of HIV-1 virus-like particles by electron cryotomography*, J. Mol. Biol., **346**(2005), pp. 577–588.

[3] J.A.G. Briggs, T. Wilk, R. Welker, H.-G. Kräusslich, S.D. Fuller, *Structural organization of authentic, mature HIV-1 virions and cores*, EMBO J., **22**(2003), pp. 1707–1715.

[4] J.A.G. Briggs, K. Grünewald, B. Glass, F. Förster, H.-G. Kräusslich, S.D. Fuller, *The mechanism of HIV-1 core assembly: Insights from three-dimensional reconstructions of authentic virions*, Structure, **14**(2006), pp. 15–20.

[5] J.A.G. Briggs, H.-G. Kräusslich, *The molecular architecture of HIV*, J. Mol. Biol., **410**(2011), pp. 491–500.

[6] I.J. Byeon, X. Meng, J. Jung, G. Zhao, R. Yang, J. Ahn, J. Shi, J. Concel, C. Aiken, P. Zhang, A.M. Gronenborn, *Structural convergence between cryo-EM and NMR reveals intersubunit interations critical for HIV-1 capsid function*, Cell, **139**(2009), pp. 780–790.

[7] D.L. Caspar, A. Klug, *Physical principles in the construction of regular viruses*, Cold Spring Harb. Symp. Quant. Biol., **27**(1962), pp. 1–24.

[8] B. Chen, R. Tycko, *Simulated self-assembly of the HIV-1 capsid: Protein shape and native contacts are sufficient for two-dimensional lattice formation*, Biophys. J., **100**(2011), pp. 3035–3044.

[9] L.S. Ehrlich, T. Liu, S. Scarlata, B. Chu, C.A. Carter, *HIV-1 capsid protein forms spherical (immature-like) and tubular (mature-like) particles in vitro: Structure switching by pH-induced conformational changes*, Biophys. J., **81**(2001), pp. 586–594.

[10] B.K. Ganser-Pornillos, A. Cheng, M. Yeager, *Structure of full-length HIV-1 CA: A model for the mature capsid lattice*, Cell, **131**(2007), pp. 70–79.

[11] B.K. Ganser, S. Li, V.Y. Klishko, J.T. Finch, W.I. Sundquist, *Assembly and analysis of conical models for the HIV-1 core*, Science, **283**(1999), No. 5398, pp. 80–83.

[12] B.K. Ganser-Pornillos, U.K. von Schwedler, K.M. Stray, C. Aiken, W.I. Sundquist, *Assembly properties of the human immunodeficiency virus type 1 CA protein*, J. Virol., **78**(2004), pp. 2545–2552.

[13] B.K. Ganser-Pornillos, M. Yeager, W.I. Sundquist, *The structural biology of HIV assembly*, Curr. Opin. Struct. Biol., **18**(2008), pp. 203–217.

[14] B.K. Ganser-Pornillos, M. Yeager, O. Pornillos, *Assembly and architecture of HIV*, Adv. Exp. Med. Biol., **726**(2012), pp. 441–465.

[15] Y. Gogotsi, *Nanomaterials Handbook*, CRC Press, (2006).

[16] J.M. Grime, G.A. Voth, *Early stages of the HIV-1 capsid protein lattice formation*, Biophys. J., **103**(2012), pp. 1774–1783.

[17] M.F. Hagan, *Modeling viral capsid assembly*, Adv. Chem. Phys., **155**(2014), pp. 1–68.

[18] J.B. Heymann, C. Butan, D.C. Winkler, R.C. Craven, A.C. Steven, *Irregular and semi-regular polyhedral models for Rous sarcoma virus cores*, Comput. Math. Meth. Med., **9**(2008), pp. 197–210.

[19] S.D. Hicks, C.L. Henley, *Irreversible growth model for virus capsid assembly*, Phys. Rev. E, **74**(2006), pp. 031912:1–17.

[20] R.W. Horne, P. Wildy, *Symmetry in virus architecture*, Virology, **15**(1961), pp. 348-373.

[21] L. Huang, C. Chen, *Understanding HIV-1 protease autoprocessing for novel therapeutic development*, Future Med. Chem., **5**(2013), pp. 1215–1129.

[22] A. Levandovsky, R. Zandi, *Nonequilibrium assembly, retroviruses, and conical structures*, Phys. Rev. Lett., **102**(2009), pp. 198102:1–4.

[23] R.V. Mannige, C.L. Brooks, III, *Tilable nature of virus capisds and the role of topological constraints in natural capsid design*, Phys. Rev. E, **77**(2008), pp. 051902:1–8.

[24] R.V. Mannige, C.L. Brooks III, *Geometric considerations in virus capsid size specificity, auxiliary requirements, and buckling*, PNAS, **106**(2009), pp. 8531–8536.

[25] R.V. Mannige, C.L. Brooks III, *Periodic table of virus capsids: Implications for natural selection and design*, PLoS One, **5**(2010), pp. e9423:1–7.

[26] T.T. Nguyen, R.F. Bruinsma, W.M. Gelbart, *Elasticity theory and shape transitions of viral shells*, Phys. Rev. E, **72**(2005), pp. 051923:1–19.

[27] T.T. Nguyen, R.F. Bruinsma, W.M. Gelbart, *Continuum theory for retroviral capsids*, Phys. Rev. Lett., **96**(2006), pp. 078102:1–4.

[28] A.S. Perelson, P.W. Nelson, *Mathematical analysis of HIV-1: Dynamics in vivo*, SIAM Review, **41**(1999), pp. 3–44.

[29] O. Pornillos, B.K. Ganser-Pornillos, B.N. Kelly, Y. Hua, F.G. Whitby, C.D. Stout, W.I. Sundquist, C.P. Hill, M. Yeager, *X-ray structures of the hexameric building block of the HIV capsid*, Cell, **137**(2009), pp. 1282–1292.

[30] O. Pornillos, B.K. Ganser-Pornillos, S. Banumathi, Y. Hua, M. Yeager, *Disulfide bond stabilization of the hexameric capsomer of human immunodeficiency virus*, J. Mol. Biol., **401**(2010), pp. 985–995.

[31] O. Pornillos, B.K. Ganser-Pornillos, M. Yeager, *Atomic level modeling of the HIV capsid*, Nature, **469**(2011), pp. 424–427.

[32] A. Pressley, *Elementary Differential Geometry*, 2nd ed., Springer, (2010).

[33] F. Sadre-Marandi, J. Liu, S. Tavener, C. Chen, *Generating vectors for the lattice structures of tubular and conical viral capsids*, Mol. Based Math. Biol., **2**(2014), pp. 128–140.
[34] A. Siber, *Continuum and all-atom description of the energies of graphene nanocones*, Nanotech., **18**(2007), pp. 375705.
[35] W.I. Sundquist, H.-G. Kräusslich, *HIV-1 assembly, budding, and maturation*, Cold Spring Harb. Perspect Med., **2**(2012), a006924
[36] R. Twarock, *Mathematical virology: a novel approach to the structure and assembly of viruses*, Phil. Trans. R. Soc. A, **364**(2006), pp. 3357-3373.
[37] M. Yeager, *Design of in vitro symmetric complexes and analysis by hybrid methods reveal mechanisms of HIV capsid assembly*, J. Mol. Biol., **410**(2011), pp. 534–552.
[38] Z. Yu, M.J. Dobro, C.L. Woodward, A. Levandovsky, C.M. Danielson, V. Sandrin, J. Shi, C. Aiken, R. Zandi, T.J. Hope, G.J. Jensen, *Unclosed HIV-1 capsids suggest a curled sheet model of assembly*, J. Mol. Biol., **425**(2013), pp. 112–123.
[39] R. Zandi, D. Reguera, R.F. Bruinsma, W.M. Gelbart, J. Rudnick, *Origin of icosahedral symmetry in viruses*, PNAS, **101**(2004), pp. 15556–15560.
[40] R. Zandi, D. Reguera, *Mechanical properties of viral capsids*, Phys. Rev. E, **72**(2005), pp. 021917:1–12.
[41] G. Zhao, J. Perilla, E. Yufenyuy, X. Meng, B. Chen, J. Ning, J. Ahn, A. Gronenborn, K. Schulten, C. Aiken, P. Zhang, *Mature HIV-1 capsid structure by cryo-electron microscopy and all-atom molecular dynamics*, Nature, **497**(2013), pp. 643–646.